

# Prediction of Incipient Damage Sites in Composites using Classifiers

ARGHAVAN LOUHGHALAM

*Department of Civil Engineering  
Johns Hopkins University, Baltimore, MD, USA*

SANJAY R. ARWADE\*

*Department of Civil & Environmental Engineering  
University of Massachusetts, Amherst, Amherst, MA, USA*

**ABSTRACT:** This paper describes a method for predicting locations in a two-phase material where effective elastic strain is concentrated above a specified threshold value by virtue of the local arrangement of phases and a specified set of boundary conditions. This prediction is made entirely based on knowledge of the material properties of the phases, their spatial arrangement, and the boundary conditions, and does not require numerical solution of the equations of elasticity. The example problem is a 2D idealization of a fiber- or particle-reinforced composite in which the fibers/particles are randomly placed in the matrix and the boundary conditions correspond to uniaxial extension. The method relies on a moving window implementation of a decision tree classifier that predicts, for all points in the material, whether the effective elastic strain will exceed a specified threshold value. The classifier operates on a set of attributes that are the coefficients of a series expansion of a discretized version of the phase geometry. The basis vectors appearing in this series expansion of the phase geometry are derived from a principal components analysis of a set of training samples for which the mechanical response is calculated using finite element analysis. These basis vectors allow the accurate representation of the phase geometry with many fewer parameters than is typical, and, because the training samples contain information regarding the mechanical response of the material, also allow prediction of the response using a classifier that takes a relatively small number of input attributes. The predictive classifier is tested on simulated two-phase material samples that are not part of the original training set, and correctly predicts whether effective elastic strain will be elevated above a specified threshold with greater than 90% accuracy.

---

\*Author to whom correspondence should be addressed. E-mail: arwade@ecs.umass.edu  
Figures 1, 2, 8, 9 and 11 appear in color online: <http://ijd.sagepub.com>

**KEY WORDS:** composites, micromechanics, stochastic mechanics, elasticity, damage initiation, classification, pattern recognition.

## INTRODUCTION

IT IS WELL understood by engineers and materials scientists that the initiation of failure in solid structures is often driven by heterogeneity at the material microscale. This has been observed experimentally since the early days of fracture mechanics, when tests showed that only when the diameter of a glass fiber became very small did the strength approach the theoretical strength calculated from first principles (Griffith, 1921). Other examples of this phenomenon include the initiation and propagation of discrete cracks in concrete materials (Hanson et al., 2004), the initiation of shear bands in soils and ductile materials (Alsaless et al., 2007; Voyiadjis and Abed, 2007), the initiation of stress-corrosion cracks at stiff inclusions in metals (Wei and Harlow, 2003), and the debonding of fiber/particle from matrix in composite materials, etc. (Ju and Lee 2001; Liu et al., 2006; Paulino et al., 2006)

Over the past several decades a rich variety of very successful computational methods have been developed for tracking the evolution of damage from the microscale to the macroscale, including fracture and fatigue analysis (Ural et al., 2005), extended finite element (Moes et al., 1999; Sukumar et al., 2000), and quasi-continuum methods (Curtin and Miller, 2003), in which the damage processes are treated as discrete discontinuities in the material, and continuum damage mechanics approaches (Kachanov, 1986; Voyiadjis and Kattan, 2006), in which the discrete damage processes are averaged over the material domain to provide estimates of the damage state without the requirement of explicitly representing the damage geometry in the computational model.

This paper presents a new method for analyzing the response of particle- or fiber-reinforced composites to loading up to the point in the load history at which damage is incipient. Specifically, the approach provides predictions of the locations at which a strain-based damage criterion is first satisfied in a 2D cross-section of a random, heterogeneous composite material subject to deterministic loads. The method adapts tools of pattern recognition, commonly used in face and character identification algorithms (Hastie et al., 2001; Witten and Frank, 2005; Vapnik, 1998), to the problem of identifying patterns in the material properties of a heterogeneous material that indicate a high likelihood of elastic strain concentration, and, therefore, if a strain-based damage criterion is used, a high likelihood of damage initiation at the site where the pattern is identified. The specific tools used are decision tree and support vector machine classifiers that are trained

using a supervised data set consisting of sample microstructures and strain fields resulting from application of a deterministic applied load. After training of the classifier, a moving window technique is implemented that allows the prediction of sites of likely incipient damage in relatively large microstructures without the need for performing an explicit mechanics analysis of the microstructural response.

In addition to describing a method for predicting sites of incipient damage, this paper also describes a robust method for reducing the dimension of the space required to describe the geometry and material properties of random heterogeneous materials. This method, based on principal components analysis of the sample microstructures, defines a set of basis functions for representing the microstructure such that an approximate representation using relatively few basis functions provides a sufficiently accurate representation of the microstructural geometry and material properties, and also reduces the number of variables to be used in classification. This dimension reduction procedure contrasts with homogenization-based methods for approximate microstructure representation (Graham et al., 2003; Kumar and Dawson, 1998) in that the basis functions preserve information about the local arrangement of the microstructural phases that is lost in homogenization schemes. This preservation of local information is particularly crucial in damage mechanics applications. The approach may find additional use in microstructural design and optimization problems (Ohser and Mücklich, 2000), in which the high dimension of the space required to describe random microstructures is a consistent obstacle to efficient problem solution.

## ANALYSIS FRAMEWORK

Let  $D \in \mathbb{R}^m$  be a domain that contains a random, heterogeneous, solid medium. Suppose that the microstructure of this medium can be described using a random vector  $X \in \mathbb{R}^n$ , the components of which describe specific properties of the microstructure. Examples include the location and shape of reinforcing particles, crystallographic orientation of constituent grains of a polycrystal, or the entries of the constitutive matrix at points in the microstructure. In cases such as the last of these, the random variables represent a discretized version of the random field describing the spatial variation of the material properties. The entries of  $X$  are chosen by the analyst according to the type of material and particular response being considered. For example, if the linear elastic response is of interest, the elastic material properties of the microstructures would be specified in  $X$ .

The microstructural response, defined as  $Y(X) = f(X)$ , cannot be evaluated analytically in most engineering applications. Typically, to evaluate  $f(X)$

approximately, numerical methods are used to solve the differential equations governing the response under a specified set of boundary conditions. The goal of this study is to present an alternative approach to achieving an approximate evaluation of  $Y(X)$  that does not rely on direct solution of the governing equations. The method uses classifiers to predict  $Y(X)$  from  $X$ , and has the advantage of being extremely computationally efficient. One significant disadvantage is that it does not seem possible to formally evaluate convergence and error of the solution, as is done for the finite element method.

The method described here includes three types of approximation that are called herein subdomain, dimension reduction, and classification approximations. Subdomain approximation can be understood by first considering a microstructure that can be described initially by an  $n$ -dimensional random vector  $X$ . One approach to evaluating the microstructural response would be to divide  $X$  into a number of  $n_s < n$ -dimensional random sub-vectors  $\{X_{s,i}\}$  and evaluate the microstructural response for each subvector. The response of the microstructural domain can be approximated using the combination of the responses of the subdomains  $\{Y_{s,i}\}$ . Practically speaking, this approach has meaning only when the subvectors represent geometric subdomains of the microstructure because, in order to make the evaluations  $\{Y_{s,i}(X_{s,i})\}$  the subvectors  $\{X_{s,i}\}$  must contain the same type of information as  $X$ . For example, if  $X$  describes the elastic modulus field throughout a material sample  $D$ ,  $\{X_{s,i}\}$  should describe the modulus throughout a subdomain  $D_{s,i} \subset D$ .

Dimension reduction approximation addresses the problem that the random vector  $X$  describing a microstructural subdomain can be of very high dimension. The high dimensionality of the microstructure descriptor poses difficulties in applying approximate techniques such as classification directly to  $X$ , and also is a major impediment to the development of microstructural design and optimization approaches that incorporate explicit representations of the material microstructure. Therefore a dimension reduction technique is used to represent the microstructure using the random vector  $\tilde{X} \in \mathbb{R}^r$  where  $r \ll n$ . This reduced dimension descriptor must be defined so that it retains most of the microstructural information that influences the response. The dimension reduction is made by defining  $\tilde{X}$  with respect to a new set of  $r$  basis vectors that are qualitatively different from, and not merely a subset of, the  $n$  basis vectors on which  $X$  is defined. Here, these basis vectors are defined by a mathematical decomposition of the random subdomain vector  $X_s$ . Because the components of  $\tilde{X}$  do not necessarily correspond to microstructural quantities such as material properties and geometry, it is not usually possible to evaluate  $Y(\tilde{X})$  directly using methods such as finite elements. Furthermore, the dimension reduction

that transforms  $X \rightarrow \tilde{X}$  introduces uncertainty into the system such that the mapping from  $\tilde{X}$  to  $Y$  is not one-to-one. Therefore an alternative function  $\tilde{Y} = \tilde{f}(\tilde{X})$  is introduced that is the approximate response calculated from the reduced order microstructural description.

An example of  $\tilde{Y} = \tilde{f}(\tilde{X})$  is a classifier that maps  $\tilde{X}$  onto a set of response classes. Consider the space  $\Omega$  including all random vectors  $\tilde{X}$ . The classifier divides this space into nonoverlapping subspaces  $\Omega_1, \Omega_2, \dots$ . These subspaces correspond to similar valued regions in  $\Omega_y$ , the response space, and are called the classes. The classes are defined using the response so that  $\tilde{X}_i \in \Omega_k$  and  $\tilde{X}_j \in \Omega_k$  implies that  $\tilde{Y}_i = \tilde{f}(\tilde{X}_i) \approx \tilde{f}(\tilde{X}_j) = \tilde{Y}_j$ , and, if the basis functions defining  $\tilde{X}$  have been chosen well,  $f(X_i) \approx f(X_j)$ . A simple class definition, used herein, involves two classes, critical and non-critical, which correspond to  $\tilde{f}(\tilde{X}) > Y^*$  and  $\tilde{f}(\tilde{X}) \leq Y^*$ , where  $Y^*$  is a threshold value of the response. For example,  $Y^*$  might be defined to be a threshold value of the effective strain corresponding to the onset of material damage.

It is shown later in this paper that dimension reduction error converges quickly to zero as the number of basis functions used for describing the microstructure is increased. The classification error, associated with the fact that the classes are defined in the space of approximate response  $\tilde{Y}$  rather than true response  $Y$ , is described and quantified in later sections. For the particular application of this study it is shown how the subdomain error can be significantly reduced by incorporating an approximate version of the long-range microstructural mechanics into the classifier.

## APPLICATION

### Problem Statement

Consider a fiber-reinforced composite in which the fibers have deterministic radius and are parallel to one another. A schematic cross section through such a material, taken perpendicular to the fiber axis, is shown in Figure 1. The loading considered in this study is transverse uniaxial extension. The loading is applied with periodic boundary conditions along the lateral edges, and the individual microstructural geometries are also considered to be periodic. The geometry and boundary conditions of the problem allow the introduction of the plane strain assumption to reduce the problem from three to two dimensions. The inclusions are distributed randomly throughout the material cross-section. A hard-core Poisson point process is used to model the centers of the inclusions. The hard core Poisson point process is defined by the intensity  $\lambda$ , and the hard core exclusion radius, which in this case is set to three times the fiber radius. The intensity governs the number of inclusions in the material sample such that the

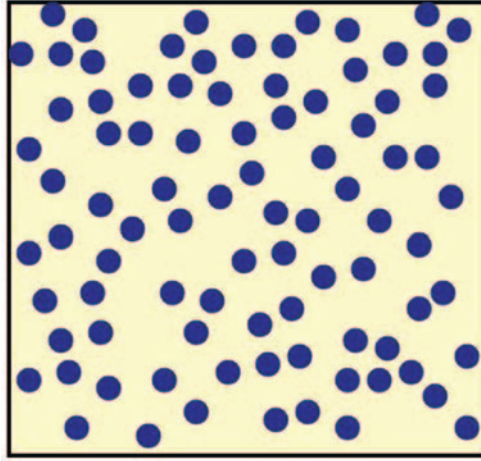


**Figure 1.** An example of a random microstructural domain.

expected number of inclusions is  $\bar{N} = \lambda A$ , where  $A$  is the area of  $D$ , the microstructural domain. The hard-core exclusion radius is set to make possible the generation of suitable finite element meshes used in the calculation of microstructural response. Details of the construction of the hard core Poisson point field are given by Stoyan et al. (1995) among others.

The elastic modulus of the inclusions is set to be three times that of the matrix,  $E_{\text{inclusion}} = 3E_{\text{matrix}}$ , and both the matrix and the inclusions are considered linear elastic and isotropic with Poisson's ratio equal to 0.3. Because only normalized versions of the strain field are used in evaluating the microstructural response, the absolute magnitudes of the elastic moduli do not affect results, rather only the ratio of the matrix and inclusion moduli determines the response. The allowable effective strain in the inclusions is five times the allowable strain in the matrix,  $\epsilon_{\text{all}}^{\text{inclusion}} = 5\epsilon_{\text{all}}^{\text{matrix}}$ . The choice of allowable effective strain is effectively arbitrary in this illustrative example, but in a practical engineering application would be chosen to correspond to the onset of material damage or degradation. This definition serves to nearly ensure that the critical locations, where elastic strain is concentrated, will occur within the matrix. In evaluating the microstructural response, the effective strain ratio is defined to be

$$\rho_e(z) = \frac{\epsilon_{\text{eff}}(z)}{\epsilon_{\text{all}}(z)} \quad (1)$$

where  $\epsilon_{\text{eff}}(z)$  is the standard effective or von Mises strain and  $z$  is a position vector in  $D$ .

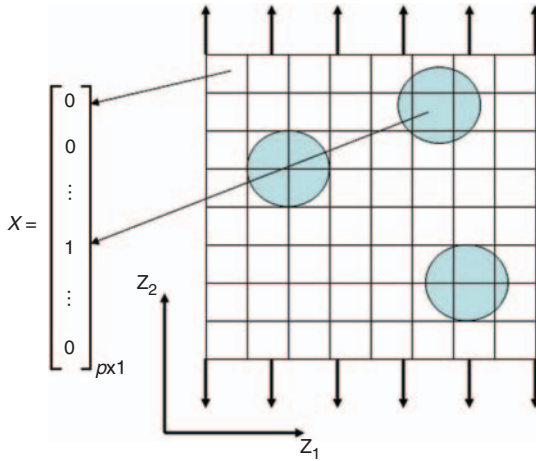


**Figure 2.** Representaion of microstructural subdomain.

The objective of the analysis described here is to predict the locations in a microstructural domain at which the effective strain ratio exceeds a specified threshold value, qualitatively corresponding to the likely onset of damage, and to do so without solving the governing equations of elasticity to obtain the strain field resulting from the applied boundary conditions and material properties. This is accomplished by applying classification to subdomains of the microstructure under consideration. In the example presented here, the microstructural domains are squares with side length equal to 40 times the fiber radius, and the subdomains are squares with side length equal to 10 times the fiber radius. The microstructural subdomains are pixelated as shown in Figure 2 so that they can be represented by a random vector, the components of which are the values of an indicator function that has value 1 in the inclusions and zero otherwise. This random vector containing the indicator function values is the high-dimensional representation of  $X_s$ , the microstructural subdomain. In the example presented here, 2500 pixels are used to describe the microstructural subdomain.

### Generating Training Data

To develop a classifier to predict the subdomain response, 1200 random, independent realizations of the synthetic microstructure described previously are generated. These microstructures, realizations of  $X_s$ , are called the training set, or training data. The microstructural subdomains are also periodic, satisfying

$$M(z_1, z_2) = M(z_1 + a, z_2) = M(z_1, z_2 + a) = M(z_1 + a, z_2 + a) \quad (2)$$

where  $M$  represents the material property field,  $z_1$  and  $z_2$  are the coordinates shown in Figure 2, and  $a$  is the length of the edge of the subdomain. The periodicity of the subdomains removes certain boundary effects, and by shifting of the microstructural geometry, allows the number of training samples to be effectively increased. This procedure is described in following sections.

The high fidelity analysis used to compute the response of the training samples, is performed using finite element analysis with the commercial code ABAQUS Pawtucket (2004). The finite element mesh is composed of 3-node, right triangular, 2D solid elements with edge length equal to one-fifth the fiber radius. Thus, the element size corresponds to the pixel size used in discretizing the microstructural material property field, and each element is assigned either the matrix or fiber constitutive properties. Although this modeling approach results in sharp discontinuities in material properties at certain element boundaries, the resulting strain fields are sufficiently smooth to allow investigation of the strain concentration effects of the fibers. The magnitude of the applied uniaxial elongation corresponds to an applied strain of 0.02.

Figure 3 shows one example result of the subdomain high-fidelity analysis. The contours represent the smoothed nodal values of the effective strain, and are shown only within the matrix. The results of the high-fidelity finite element analysis shows that in most of the samples, the maximum effective strain ratio is located between two closely spaced inclusions that are

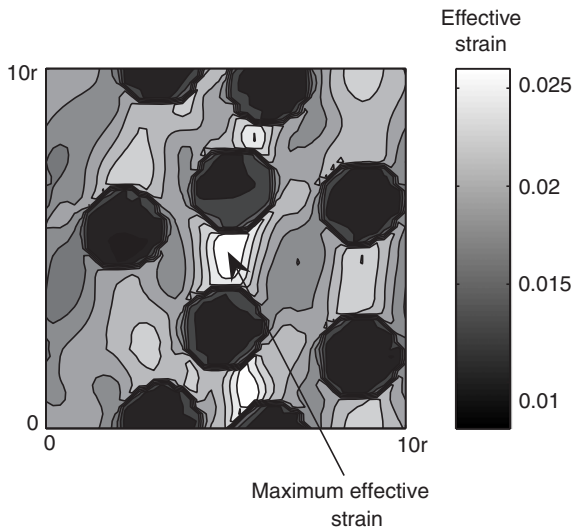


**Figure 3.** Effective strain contour. The maximum of effective strain in the subdomain occurs between two close inclusions in the direction of applied load.

aligned in the direction of applied displacement. The 1200 training samples yield maximum effective strain ratios with mean 23.5 and variance 2.18.

### Classification of Training Samples

In order to use the training samples in establishing a reduced order representation  $\tilde{X}_s$  of  $X_s$ , and in training of a classifier, the training samples must themselves be classified according to some criterion involving the microstructural response. Here, two classes are defined, corresponding to critical and noncritical microstructural configurations, respectively. In defining the response classes, a threshold level,  $\rho_{\epsilon_{th}}$ , of the effective strain ratio, is defined. Although in this example the threshold is somewhat arbitrary, set to the mean plus one standard deviation of the maximum effective strain ratio, in a practical engineering context it would be chosen to correspond to the strain at which damage initiates, perhaps adjusted by a factor of safety. Based on this threshold value of the maximum effective strain ratio, the training data are divided into classes by the following criteria:

- A subdomain is considered critical if the maximum effective strain ratio is above the threshold,  $\rho_{\epsilon} > \rho_{\epsilon_{th}}$ , and is located at the center of the random subdomain.
- A subdomain is considered non-critical if the above condition is not met.

Both location and magnitude of the maximum effective strain ratio are used in the classification since the eventual goal of the approach is to identify locations within the microstructure where large strain localizations occur, not merely to determine whether large strain localization occurs somewhere within the microstructure. Because the probability of the maximum effective strain ratio occurring exactly at the center of the subdomain is zero, all of the training samples are initially classified as noncritical.

The set of critical samples is generated by making use of the periodicity of the microstructure as follows. For those training samples for which  $\rho_{\epsilon} > \rho_{\epsilon_{th}}$  let the coordinates of the point where the maximum effective strain ratio occurs be  $z_{1, \epsilon_{max}}$  and  $z_{2, \epsilon_{max}}$ . The material property field of the corresponding critical training sample is then given by

$$M^*(z_1, z_2) = M(z_1 - z_{1, \epsilon_{max}}, z_2 - z_{2, \epsilon_{max}}), \quad (3)$$

which is then pixelated to deliver  $\{X_{s, \text{crit}, i}\}$  the set of critical training subdomains. Effectively, the periodic microstructure is shifted so that the location of the maximum effective strain ratio is at the center of the microstructural subdomain. Although this method of generating the training sets results in the critical and noncritical samples being nonindependent, the

efficiency of the generation is greatly improved, and sufficient samples are generated so that nonindependence does not significantly compromise the approach. Of the total of 1200 training samples, 141 have maximum effective strain ratio exceeding the threshold, and are transformed according to Equation (3) to form the set of critical training samples.

### Basis Function Extraction and Microstructure Representation

In order to achieve the dimension reduction described above for the composite material being studied here, principal component analysis is used to derive a set of basis vectors for representation of the microstructural subdomains. Using principal component analysis to calculate the basis vectors assures that the geometry of the microstructural subdomains can be captured with a minimum number of basis vectors, thereby achieving the greatest possible dimension reduction. No such assurance is available, however, that basis vectors obtained by principal components analysis will best serve as attributes in the developed classifier. The investigation of the choice of basis vectors for use in classification is a topic of ongoing research, and is beyond the scope of the current paper. Results shown in the following, however, indicate that the basis vectors obtained from principal components analysis perform very well in classification.

The following procedure is followed in extracting the basis functions. First, the random vectors representing the training samples are transformed, under the assumption of stationarity, to have zero mean, by  $\hat{X}_s = X_s - E[X_s]$ . The implicit assumption of stationarity in this calculation is consistent with the construction of the random microstructures, which are based on a spatially homogeneous Poisson point field. Next, a matrix  $F$  is constructed that has  $\hat{X}_{s,i}$ ,  $i = 1, \dots, p$  as its columns, where  $p$  is the number of samples in the training set, 1200 for the set of noncritical microstructures and 141 for the set of critical microstructures. The covariance matrix of the microstructural subdomains is estimated by

$$C_M = \frac{1}{p-1} FF^T. \quad (4)$$

The eigenvectors of  $C_M$ , denoted by  $e_i$ , and the corresponding eigenvalues  $\lambda_i$  are calculated and form the basis for representation of the microstructural subdomains (Johnson and Wichem, 2002). These eigenvectors are the principal components of the microstructural subdomains. It should be noted that the dimension of  $F$  is  $2500 \times 1200$  for the non-critical set and  $2500 \times 141$ , resulting in covariance matrices that are rank-deficient so that at most 1200 and 141 independent eigenvectors exist for the noncritical and

critical classes, respectively. It is shown in the following that, since the microstructural subdomains can be accurately represented by linear combinations of a relatively small number of basis vectors, this rank-deficiency does not pose practical obstacles to implementation of this approach.

Figure 4 shows the eigenvalues of the noncritical and critical classes in descending order. The main observation to be made from this figure is that the eigenvalues of the principal components decay quickly to zero. For both classes the first 100 principal components capture upwards of 98% of the total variance of the microstructural subdomains. This observation supports the contention that the rank-deficiency of the covariance matrices does not significantly affect the results, and also suggests that dimension reduction is possible by using only the first few tens of basis vectors in representing the microstructural subdomains.

Figure 5 shows the sample mean and the first two basis vectors for the critical data set. To generate this figure the  $50 \times 50$  pixel microstructural

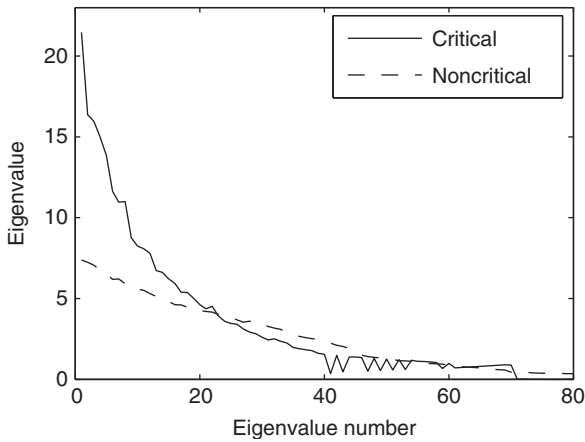


Figure 4. Eigenvalue decay for noncritical and critical training classes.

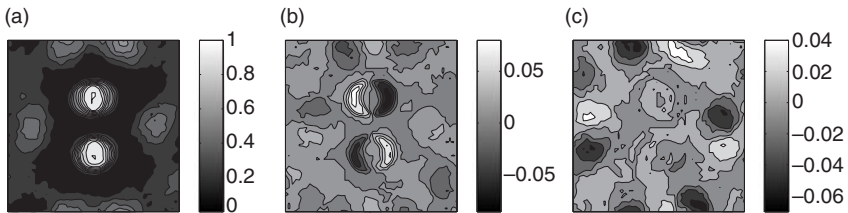


Figure 5. Mean value and first two basis functions of critical subdomains (a) mean value, (b) first basis function, (c) second basis function.

subdomain has been reconstructed from the  $2500 \times 1$  basis vectors. The sample mean shows the underlying geometry of the critical samples, with two inclusions closely spaced and aligned with the principal load direction. This structure is also evident in the first basis vector, but by even the second basis vector the obvious connection to the microstructural geometry is lost. It is shown in succeeding sections that even basis vectors that do not have an obvious connection to the microstructural geometry contain information that is useful in classifying the microstructural response.

The eigenvectors of the microstructure covariance matrix form a basis for the 2500 dimensional vector space in which the vectors defining the microstructural subdomains are described. If the eigenvectors are sorted according to descending order of their corresponding eigenvalues a microstructural subdomain can be approximately represented by

$$X_s \approx \tilde{X}_s = \frac{\mu X_s}{\mu X_s} + \sum_{i=1}^r d_i e_i \quad (5)$$

in which  $d_i = \hat{X}_s \cdot e_i$  is the projection of the mean zero microstructure vector onto basis vector  $e_i$  and  $\mu_{X_s}$  is the mean of the microstructure vector. If the series is truncated so that  $r \ll p$  then an approximate reduced order representation of the microstructure is obtained that converges to the exact microstructure according to  $\lim_{r \rightarrow p} \tilde{X}_s = X_s$ . The representation of Equation (5) gives a microstructural subdomain vector  $\tilde{X}_s$  in which each component is a real valued number, whereas the true microstructure vectors have components that are binary, taking values of zero or one. To improve the accuracy of the reduced order representation, the components of the reduced order representation shown above are rounded to obtain a microstructure vector with binary components according to

$$[\tilde{X}_s]_i = \begin{cases} 1 & \text{if } [\tilde{X}_s]_i \geq 0.5 \\ 0 & \text{otherwise} \end{cases} \quad (6)$$

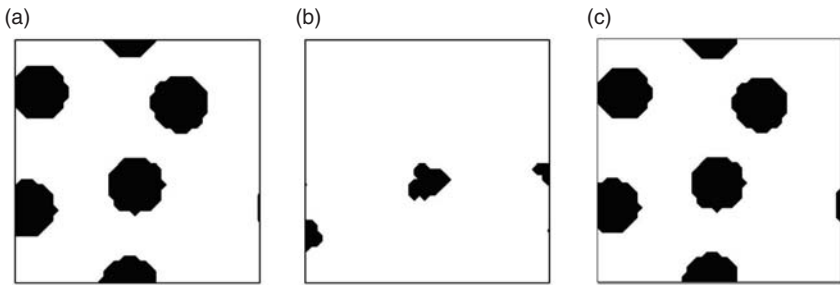
in which  $[\tilde{X}_s]_i$  is the  $i$ -th component of  $\tilde{X}_s$ .

Figure 6 shows a sample microstructure, represented on a  $50 \times 50$  grid of pixels, along with the approximate representations defined by Equations 5 and 6 with  $r = 10$  and  $r = 20$ , and using the basis vectors extracted from the noncritical members of the training set. This example shows that a high quality representation is available with relatively few basis vectors. Effectively, the microstructure description is given by the

$r$  coefficients  $d_i = \hat{X}_s \cdot e_i, i = 1, \dots, r$ . To state this result quantitatively, define the representation error to be

$$Err_s = ||\tilde{X}_s - X_s||. \tag{7}$$

This error, estimated from 100 randomly generated microstructures, decays with an increase in the number of terms in the representation (Figure 7). For this particular microstructure the representation is extremely accurate when 50 basis vectors are included. In the following, it is shown that even fewer than this many basis vectors may provide a representation suitable for accurate response classification.



**Figure 6.** Reduced order representations of microstructural subdomains (a) target microstructure, (b) 10 basis vectors, (c) 50 basis vectors.

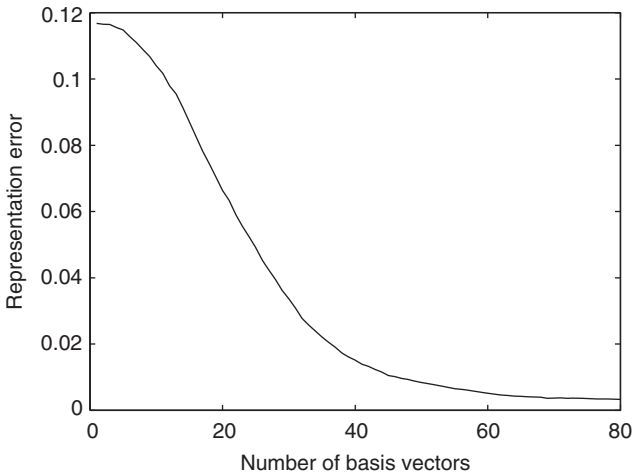


**Figure 7.** Microstructure representation error decay with inclusion of additional basis vectors.

## Classification

A classifier is a function that maps a set of independent input variables onto a set of classes. In the context of the current micromechanics problem, the input variables describe the microstructural geometry and the two classes correspond to critical or noncritical microstructural response. The classifier  $C(X_s)$  maps the microstructural subdomain vector onto the response classes  $C_1, C_2$ . Here, critical microstructures are classified as belonging to  $C_1$  and noncritical microstructures to  $C_2$ .

In practice, classifying the microstructures based on the raw microstructure vectors  $X_s$  is inefficient and inaccurate due to the high dimensionality of  $X_s$ . Therefore, using the reduced order description described above, an approximate classifier  $\tilde{C}(\tilde{X}_s)$  is derived that takes as its input variables the coefficients  $d_i$  of the reduced order representation of Equation 5. Here, two types of classifier, a decision tree and a support vector machine are described and trained using the training samples already introduced for basis vector extraction.

### DECISION TREE CLASSIFIERS

A classification tree is a directed graph model consisting of a finite set  $N = \{n_1, n_2, \dots, n_k\}$  whose elements are called nodes and a set of ordered pairs of nodes called edges that connect two nodes to each other. The node on the highest level is called the root node, and the nodes at the lowest level of the tree are called the leaves. Every node except the leaves is connected to nodes at a lower level that are called children, and every node except the root is connected to a node at a higher level that is called a parent. Each node contains a binary logical operator evaluating one of the input variables. The leaves contain assignments to a particular class. In the current application, the input variables are the representation coefficients  $d_i$  and the classes are  $C_1 = \text{critical}$  and  $C_2 = \text{noncritical}$ .

There exist a variety of established algorithms for deriving a decision tree from a set of training data and assigned classes. The algorithm used here is the C4.5 algorithm (Kohavi and Quinlan, 2002) that attempts to maximize the gain ratio at each node. One problem that can arise when deriving a decision tree from data is overfitting. An overfit decision tree contains too many nodes, and, although it achieves very high accuracy in placing the training data into the correct classes, it may perform very poorly when asked to classify sets of input variables not drawn directly from the training set. The C4.5 algorithm prunes the decision tree resulting from gain ratio maximization to overcome the problem of overfitting.

Here, the decision tree classifier is trained using the set of 1200 noncritical and 141 critical training samples. It is found that using only 20 input

variables,  $d_i, i = 1, \dots, 20$ , obtained by projection of the microstructure onto the noncritical basis vectors, provides very high classification accuracy as well as efficient classification as manifested in a relatively compact decision tree. The inclusion of additional input variables  $d_i, i = 21, \dots$  is found to have negligible effect on the accuracy of the decision tree. It is possible to achieve such high classification accuracy using only 20 input variables because the basis vectors have been extracted using principal components analysis. Note that the 20 variables required for accurate classification is significantly fewer than the 50 required for accurate geometric representation.

In order to test the accuracy of the classifier a 10-fold cross validation test is performed. In a 10-fold cross validation the training data set is divided into 10 subsets containing equal numbers of samples, and sequentially one subset is used to test the classifier trained by the remaining nine subsets. The cross validation accuracy is the percentage of the data which are correctly classified (Sundararaghavan and Zabarar, 2005).

A number of decision trees are constructed using the program WEKA with a variety of control parameters (Witten and Frank, 2005). Of those investigated, the best performing decision tree is constructed by limiting the number of training samples assigned to each leaf to one for initial tree construction, and then pruning the tree using a pessimistic pruning algorithm with confidence factor 0.25. The resulting, heavily pruned, decision tree has 24 leaves and gives a net accuracy, estimated by 10-fold cross validation, of 98.06%. The confusion matrix for the decision tree classifier is shown in Table 1. All confusion matrices shown are computed from 10-fold cross validation on the 1200 training samples. This type of classifier is referred to from here forward as a Near Field Decision Tree classifier (NF DT) because the input variables quantify only the geometry of the microstructural subdomain, which, in the moving window approach described later, corresponds only to the portion of the microstructural domain within the current window. If prediction of critical response is considered a positive result, the false positive and false negative error rates of the decision tree are 1.1 and 9.2%, respectively. Although the total accuracy of the classifier is high, the false negative error rate is higher than would be desired in an engineering application since false negative

**Table 1. Confusion matrix for NF DT.**

<b>True class</b>	<b>Classified as noncritical</b>	<b>Classified as critical</b>
Noncritical	1187	13 (1.1%)
Critical	13 (9.2%)	128

errors are unconservative. Finding methods for decreasing the false negative error rate is a topic of current investigation (Tan and Arwade, 2008).

### *SUPPORT VECTOR MACHINE*

A support vector machine (SVM) is a classification method that provides an alternative to the decision tree classifier described in the previous section that has shown promising empirical results in many applications such as handwriting recognition and text categorization (Vapnik, 1998). SVMs also perform particularly well when the dimension of the input data is very high (Tan et al., 2005). The general idea of an SVM is, as in the case of a decision tree classifier, to predict the class to which a point in the input data space belongs. Instead of using a series of logical operations on the input variables, as in the decision tree classifier, in the SVM approach a hyperplane is defined in the input data space that separates the two classes with a minimum of misclassifications. There are three types of input data that require somewhat different treatment within the SVM approach, linear separable data, linear nonseparable data, and nonlinear separable data. The training data developed here are linear nonseparable. Since the linear nonseparable case is an extension of the linear separable case, brief descriptions of both are provided.

#### *Linear Separable Case*

Figure 8 shows a data set in a 2D input data space containing observations  $x_i$  belonging to two different classes  $C_1$  and  $C_2$ . The data are linear separable if there exists a hyperplane that divides the input data space into two regions  $\omega_1$  and  $\omega_2$  such that

$$C(x_i) = C_1 \rightarrow \mathbf{x}_i \in \omega_1, \quad (8)$$

$$C(x_i) = C_2 \rightarrow \mathbf{x}_i \in \omega_2, \quad (9)$$

with no error. The figure illustrates that the definition of this hyperplane, the decision boundary, is not, in general, unique. The classifier performs best in classifying observations that are not part of the training set if the margin, the distance from the separating hyperplane to the nearest observations, is maximized (Tan et al., 2005).

The decision boundary can be written as  $w \cdot x + b = 0$ , in which the parameters  $w$  and  $b$  are chosen so as to maximize the margin. Thus, the operation of classification is reduced to the simple algebraic operation of determining on which side of the decision boundary an observation lies. This evaluation can be substantially more efficient than evaluation of the large number of logical operations in a decision tree with many nodes.

*Non-separable case*

Figure 9 shows a case in which the data are not linearly separable. Even in this case, it is possible to construct a decision boundary that is optimal in the sense that now, instead of simply maximizing the margin, a tradeoff must be

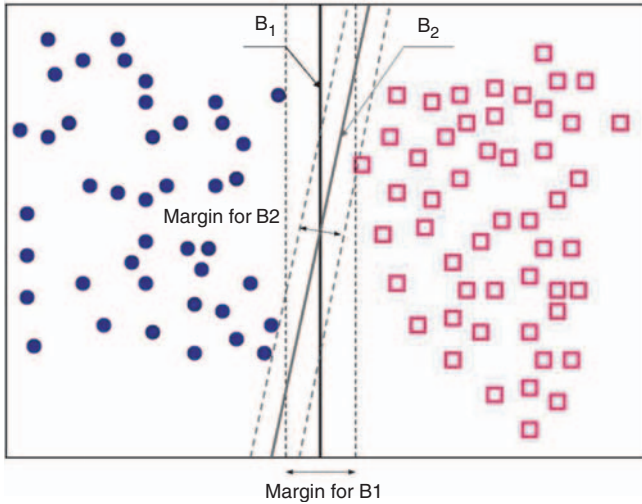


**Figure 8.** Decision boundaries (after Tan et al., 2005).

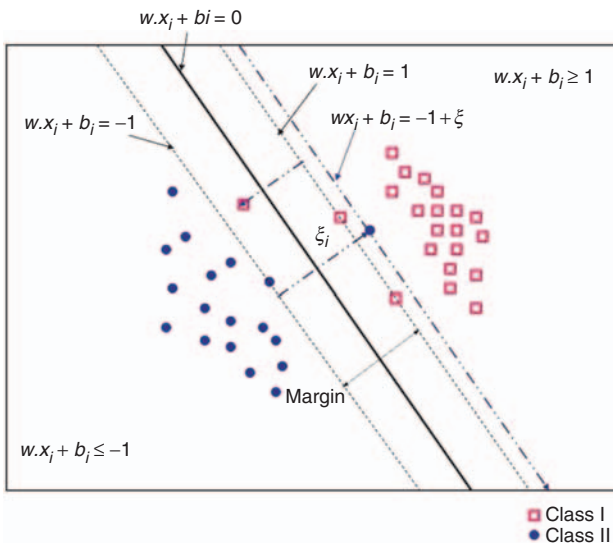


**Figure 9.** Support vector machine for nonseparable case [after Sundararaghvan and Zabaras (2005) and Tan et al. (2005)].

considered between the margin width and the training error. Choice of the appropriate decision boundary reduces to a constrained optimization problem solved using Lagrange multipliers. Once the optimal decision boundary has been obtained, it can be expressed in the same form as for the linear separable case, and the classification operation again reduces to determining on which side of the decision boundary an observation lies.

### *SUPPORT VECTOR MACHINE CLASSIFIER*

An SVM classifier is trained on the same training data as used to train the decision tree classifier described previously. These training data are linearly nonseparable. This classifier, which takes as input the representation coefficients  $d_i$ , which quantify only the local material arrangement, is called the Near Field Support Vector Machine (NF SVM). The NF SVM classifier is trained using the software package WEKA (Witten and Frank, 2005) which uses sequential minimal optimization (SMO) (Platt, 1999) to solve the optimization problem that leads to the appropriate choice of decision boundary. Table 2 shows the confusion matrix for the NF SVM classifier, which yields a total accuracy of 94.85% and false positive and false negative rates of 2.92 and 24.11% respectively. In comparison to the NF DT classifier, the overall performance of the NF SVM is slightly worse in terms of the total accuracy and false positive rate, but significantly worse in terms of the false negative rate, which is 9.22% for the NF DT classifier. The performance of the near field classifiers is summarized in Table 3.

### **Near Field Moving Window Classification**

In this section, a moving window technique is used to extend the classifier approach developed in the preceding to predict the locations where strain

**Table 2. Confusion matrix for NF SVM.**

<b>True class</b>	<b>Classified as noncritical</b>	<b>Classified as critical</b>
Noncritical	1165	35 (2.9%)
Critical	34 (24%)	107

**Table 3. Compare classification error for different classifiers.**

<b>Classifier</b>	<b>Overall error (%)</b>	<b>False positive error (%)</b>	<b>False negative error (%)</b>
NF DT	1.9	1.1	9.2
NF SVM	5.2	2.9	24

concentration is likely to occur in a microstructure that is qualitatively similar to the training microstructures, but is substantially larger. Here, the larger microstructures are square with side length of 40 times the fiber radius. The moving window is a square with side length equal to 10 times the fiber radius, and is the same size as the training samples. The moving window algorithm is defined as follows.

Let  $z_i$  be a position in the large microstructural domain described by the microstructure vector  $X$  that lies at the corner of a pixel used in defining the random vector representation of the microstructure. This point defines the center of a microstructural subdomain described by  $X_{s,i}$  that is a square with side length of 10 times the fiber radius and contains 2500 square pixels. The classifier developed previously is applied to  $X_{s,i}$  and provides a prediction of whether the effective strain ratio at  $z_i$  exceeds the threshold value. The moving window classification, in which each pixel corner in  $D$  is treated as the center of a microstructural subdomain, produces a binary response field  $C_w(z)$ . In this binary response field,  $C_w(z_i) = 1$  indicates that subdomain  $X_{s,i}$  has been classified as critical.

Figures 10(a) and (b) show the result of moving window classification on a single realization of  $X$ , using the NF DT and NF SVM classifiers, respectively. The white regions are regions in which  $C_w = 1$ , that is, the subdomains centered at points colored white in the figures are classified as critical. No moving window classification is possible for points that are closer than five fiber diameters to the boundary of  $D$  since a full-sized microstructural subdomain cannot be defined that is centered at these locations. For comparison, the effective strain ratio field as determined by finite element analysis is converted to a binary field using a threshold value of the effective strain ratio. This binary field, shown in Figure 10(c), indicates regions in which the effective strain ratio exceeds the threshold by white.

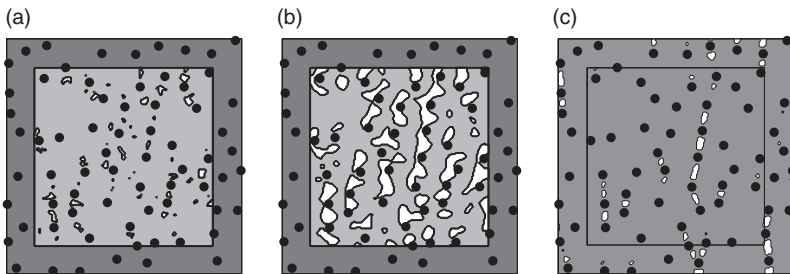


**Figure 10.** Critical regions of microstructure using moving window classification or finite element analysis: (a) NF DT, (b) NF SVM, (c) FEA.

The confusion matrices for the NF DT and NF SVM classifier (Table 1 and 2) show that the false positive rate for the NF SVM classifier is essentially twice that of the NF DT classifier. This is manifest in the moving window results, which show that the NF SVM classifier predicts a dramatically higher proportion of the microstructural domain to be critical.

The differences between the predictions of the NF DT and NF SVM classifiers [Figure 10(a) and (b)] can be quantified using the same vocabulary as is used in the confusion matrices described above. For the moving window classifications, the total error is the fraction of  $D$  in which the classifier and finite element results disagree. The false positive error is the fraction of the area that is classified as critical that is not critical in the finite element result, and the false negative error is the fraction of the area that is classified as noncritical that is critical in the finite element result. Table 4 shows the error rates for the NF DT and NF SVM classifier in moving window implementation. The results of Table 4 are based on analysis of 150 samples. The results show that the performance of both classifiers degrades when implemented in a moving window algorithm. The quantitative performance of the NF DT classifier is considerably better than the NF SVM classifier, though qualitative inspection of Figure 10(a), (b), and (c) shows that the NF SVM classifier performs poorly by severely overpredicting the region of the sample that is critical, which is a conservative error, but one which severely reduces the information gained by application of the classifier.

### **Inclusion of Far-field Material Effects**

The results of the moving window classification presented in the previous section show clearly that the near field pattern recognition algorithms, taking as input only the reduced order representation of the local microstructural geometry, are inadequate for identifying sites of strain concentration in fiber-reinforced composites subject to transverse uniaxial load. Two possible approaches to improving the performance of the classifier are: (1) to increase the number of input variables considered by the classifier, that is, to include more than 20 coefficients from the approximate

**Table 4. Compare moving window classification error for classifiers.**

<b>Classifier</b>	<b>Overall error (%)</b>	<b>False positive error (%)</b>	<b>False negative error (%)</b>
NF DT	5.40	3.06	18.59
NF SVM	27.84	28.15	5.37

representation of the classifier [Equation (5)], or (2) increase the size of the moving window so that a larger local material subdomain is considered in making response predictions. As stated previously, the inclusion of additional input variables does not significantly improve classifier performance. In general, an increase in the number of input variables may actually degrade classifier performance due to resultant overfitting of the classifier. Increasing the size of the moving window, on the other hand, while it should result in improved performance, results in a significant reduction of efficiency due to the increased domain size.

Here, an alternative approach is introduced that relies on a heuristic incorporation of the effect of the microstructure in the far field on the local effective strain ratio through a single additional input variable. Consider Figure 11, showing the moving window, with side length  $a$ , at a particular location in the microstructure and the applied uniaxial elongation  $\delta$ . If the material domain were occupied by a homogeneous isotropic material the strain at all locations would be simply  $\epsilon_{\text{avg}} = \delta/L$ . If, as is the case in the example material of this study, the material is heterogeneous in its elastic properties, the strain field itself becomes heterogeneous. In the example material considered here, the fiber inclusions are much stiffer than the matrix. If regions  $S_1$  and  $S_2$  contain more than the expected number of inclusions, the effective stiffness of these regions will in turn be higher than expected, and the average strain in the moving window subdomain, denoted

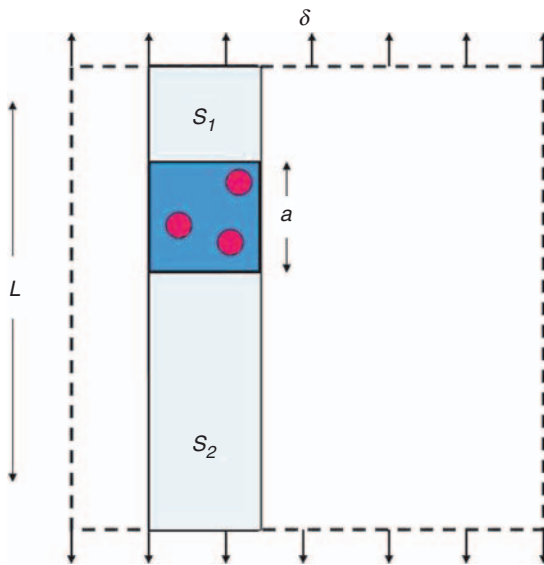


Figure 11. A strip of microstructure including the moving window.

by  $\hat{\epsilon}$ , would be expected to be greater than  $\epsilon_{\text{avg}} = \delta/L$ . Conversely, if  $S_1$  and  $S_2$  contain fewer than the expected number of fiber inclusions it would be expected that  $\hat{\epsilon} < \epsilon_{\text{avg}}$ . This uncertainty in the average strain within the moving window subdomain is the main contributor to loss of classifier accuracy when implemented in a moving window algorithm. Essentially, the boundary conditions applied to a window do not correspond to those used to generate the training data used in training the classifier.

Assuming that the effective elastic modulus within the moving window subdomain is equal to the ensemble average Voigt average elastic modulus of the microstructure  $E_v$ , the average strain in the moving window subdomain is given approximately by

$$\hat{\epsilon} = \frac{\delta}{((L - a)E/E_s) + a} \quad (10)$$

where  $E_s$  is the Voigt average elastic modulus of the material occupying  $S_1$  and  $S_2$ .

This average strain in the moving window subdomain,  $\hat{\epsilon}$ , is a random variable by virtue of the uncertainty in  $E_s$  brought on by the Poisson hard-core field model for the inclusion locations. A Monte Carlo simulation of 100,000 samples of  $E_s$ , and subsequent computation of the corresponding values of  $\hat{\epsilon}$  yields a probability mass function (pmf) with mean value  $2.0e-2$ , and standard deviation  $8.6e-4$ . The skewness of the data is 0.20 and the kurtosis is 3.03 indicating that the distribution is close to Gaussian, but with a small positive skewness.

To incorporate information about the far-field material properties into the classifier, a new set of training data is generated in which the training samples are subject to a uniaxial deformation corresponding to a random average strain  $\hat{\epsilon}$  that is drawn from the empirical pmf estimated as described above. Because the response considered here is linear, the finite element simulations used to generate the original training set can be reused by performing the following operations:

1. Generate a sample of  $\hat{\epsilon}$  from the empirical pmf,
2. Compute the effective strain field in the training sample by  $\hat{\epsilon}_{\text{eff}}(z) = (\hat{\epsilon}/\epsilon_{\text{avg}})\epsilon_{\text{eff}}(z)$ , where  $\epsilon_{\text{eff}}$  is the effective strain field determined by finite element analysis for an applied uniaxial elongation corresponding to  $\epsilon_{\text{avg}} = 0.02$ .

At this point the 1200 training samples are divided into classes as previously, with the difference that the set of input variables to the classifier now consists of the first 20 principal components and the average applied strain  $\hat{\epsilon}$ . This single additional input variable is designed to provide an

approximate characterization of the effect of the far-field material properties on the state of strain in the training sample.

Using this training data, both a decision tree and support vector machine classifier are trained using the same procedures and software as described previously. These classifiers are here called the NF FF DT and NF FF SVM classifiers, where the ‘FF’ stands for ‘far field’. As with the NF DT and NF SVM classifiers accuracy is evaluated using 10-fold cross validation on the 1200 training samples, the results of which are shown in Table 5 and 6, and are summarized in Table 7, which also shows the 10-fold cross validation accuracies for the NF DT and NF SVM classifiers. These results show that the decision tree classifier performs significantly worse when uncertainty in the applied deformation is included in the training samples. The worsening of performance is particularly striking in the false negative error rate, which jumps from 9% to 21%. The support vector machine classifier, on the other hand, performs better in classifying the training samples that include deformation uncertainty. This is an indication that the NF FF SVM classifier may provide significantly improved performance in a moving window context.

The goal of including the effects of the far-field microstructure is to improve the performance of the moving window classifier at predicting

**Table 5. Confusion matrix for NF FF DT.**

True class	Classified as noncritical	Classified as critical
Noncritical	1037	18 (1.7%)
Critical	31 (21%)	114

**Table 6. Confusion matrix for NF FF SVM.**

True class	Classified as noncritical	Classified as critical
Noncritical	1041	14 (1.3%)
Critical	16 (11%)	129

**Table 7. Compare classification error for different classifiers.**

Classifier	Overall error (%)	False positive error (%)	False negative error (%)
NF DT	1.9	1.1	9.2
NF SVM	5.1	2.9	24
NF FF DT	4.1	1.7	21
NF FF SVM	2.5	1.3	11

locations of strain concentration in large microstructures. In order to implement the NF FF DT and NF FF SVM classifiers as moving window classifiers, an estimate of  $\hat{\epsilon}$  must be obtained. This is accomplished through Equation (10), in which  $E_s$  is replaced by the Voigt average elastic modulus of regions  $S_1$  and  $S_2$  that are determined by the current position of the moving window.

Example results of the moving window classification using the NF FF DT and NF FF SVM classifiers are shown in Figure 12, and numerical results generated from 150 samples are shown in Table 8. The figure shows that the NF FF DT performs poorly, and the inclusion of the far-field material characteristics in the classification scheme results in essentially no improvement in performance. The NF FF SVM classifier, on the other hand, yields a quite satisfactory classification. Although the total area classified as critical is substantially smaller than indicated by the finite element result, the location of the critical regions corresponds quite closely to the finite element result. The quantitative results of Table 8 shows that for the SVM classifier the inclusion of the far-field effect results in a dramatic decrease in the false positive error, and a corresponding increase in the false negative error. Because the critical area is only a small fraction of the total area of the microstructural domain, the total accuracy of the NF FF SVM classifier is substantially better than that of the NF SVM

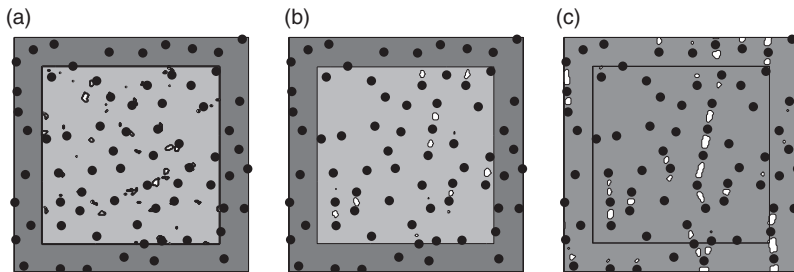


**Figure 12.** critical regions of microstructure using moving window classification or finite element analysis: (a) NF FF DT, (b) NF FF SVM, (c) FEA.

**Table 8. Compare moving window classification error for classifiers.**

Classifier	Overall error (%)	False positive error (%)	False negative error (%)
NF DT	5.4	3.1	18
NF SVM	28	28	5.4
NF FF DT	5.6	3.7	94
NF FF SVM	1.9	0.39	39

classifier in a moving window implementation. One outstanding question is how best to quantify the performance of the moving window classifiers. Visual inspection of Figure 12 indicates that the performance of the NF FF SVM classifier is satisfactory, yet this conclusion is not supported by the very high false negative error rate shown in Table 8. One approach that is currently being investigated is to use clustering techniques to assess whether the classifier correctly identifies the locations, if not the sizes, of the critical regions.

## CONCLUSION

For the problem of identifying sites of elastic strain concentration in a 2D cross-section of a fiber-reinforced composite subject to deterministic, transverse, uniaxial loading, a support vector machine classifier, implemented in a moving window scheme, is able to predict sites of strain concentration with an accuracy of greater than 95%. The classifier operates on a set of microstructural descriptors that are obtained by projecting the microstructure onto a set of basis functions that are obtained by principal components analysis of the training samples. Simulation results indicate that, for this particular application, a support vector machine classifier performs significantly better than a decision tree classifier trained on the same set of training data. Despite the limitations imposed on these conclusions by the highly simplified character of the problem studied, this use of pattern recognition techniques to solve mechanics problems, along with recent work by the current research team (Arwade, 2006; Loughalam et al., 2006; Liu et al., 2007; Tan and Arwade, 2008), constitutes, to the authors knowledge, the first times that classifiers and pattern recognition algorithms have been used to obtain predictions of the mechanical response of solids to loads without the solution of the governing equations.

The example given here of the application of classification to micro-mechanics problems is essentially a proof-of-concept, and suffers from the following limitations. The predicted response is elastic strain concentration, and therefore does not actually capture any of the response of the material once damage has begun to occur. Even this prediction of elastic response may prove useful in identifying sites within a random heterogeneous material at which damage is likely to initiate due to the wide acceptance of strain-based criteria for damage initiation. Once such sites have been identified using the classifier, it should be possible to simulate the actual initiation and evolution of damage using established damage mechanics models. The knowledge of the location of likely damage initiation provides the opportunity to deploy computational resources (mesh refinement, cohesive elements, multiscale formulations) only in those regions of the studied body in which they are

likely to be necessary. The classifier shown here is valid only for the specific example microstructure shown, subject to uniaxial loading. Indeed the only uncertainty in the problem is the location of the inclusions. Ongoing research seeks to extend the application of classifiers to other materials such as ductile polycrystalline materials, to develop classifiers that can account for uncertainty in loading, and finally to develop classifiers that directly predict the onset of nonlinear damage responses, such as fracture, material phase debonding, and plastic strain localization.

An ancillary benefit of the work presented here is the development of an efficient dimension reduction technique for material microstructures. In the example shown here, the random microstructure, originally described by 2500 components of a random vector, is shown to be well represented by 20 coefficients of a series expansion of the microstructural geometry in a set of basis functions obtained by principal components analysis. This dimension reduction approach is generally applicable to any material in which the material properties exhibit spatial variation, and the benefits would be expected to be even more dramatic when applied to richer microstructures such as polycrystals or functionally graded materials. While this dimension reduction procedure is crucial to the success of the classification presented here, it also has potential application in material design and optimization problems, in which the search space is often of very high dimension, thereby hindering the application of traditional design and optimization approaches.

### ACKNOWLEDGEMENTS

The authors acknowledge the financial support of the U.S. National Science Foundation under grant #0423582. Discussions with Prof. T. Igusa of Johns Hopkins University's Department of Civil Engineering were very valuable to the completion of this work.

### REFERENCES

- Alsaleh, M.I., Voyiadjis, G.Z. and Alshibli, K.A. (2007). Modeling Strain Localization in Granular Materials Using Micropolar Theory: Mathematical Formulations, *International Journal for Numerical and Analytical Methods in Geomechanics*, **30**(15): 1501–1524.
- Arwade, S.R. (2006). Reduced Order Descriptors for Random Composite Microstructure In: Spanos, P. and Deodatic, G. (eds), *Proceedings of the Fifth Computational Stochastic Mechanics Conference*, Rhodes, Greece, 21–23 June.
- Curtin, W.A. and Miller, R.E. (2003). Atomistic/Continuum Coupling in Computational Materials Science, *Modelling and Simulation in Materials Science and Engineering*, **11**(3): R33–R68.
- Graham, L.L., Gurley, K. and Masters, F. (2003). Non-Gaussian Simulation of Local Material Properties based on a Moving-window Technique, *Probabilistic Engineering Mechanics*, **18**(3): 223–234.

- Griffith, A.A. (1921). *Royal Society of London Philosophical Transactions Series A*, **221**: 163.
- Hanson, J.H., Bittencourt, T.N. and Ingraffea, A.R. (2004). Three Dimensional Influence Coefficient Method for Cohesive Crack Simulations, *Engineering Fracture Mechanics*, **71**(15): 2109–2124.
- Hastie, T., Tibshirani, R. and Friedman, J. (2001). *The Elements of Statistical Learning*, Springer, New York.
- Johnson, R.A. and Wichern, D.W. (2002). *Applied Multivariate Statistical Analysis*. Prentice Hall, New Jersey.
- Ju, J.W. and Lee, H.K. (2001). A Micromechanical Damage Model for Effective Elastoplastic Behavior of Partially Debonded Ductile Matrix Composites, *International Journal of Solids and Structures*, **38**(36–37): 6307–6332.
- Kachanov, L.M. (1986). *Introduction to Continuum Damage Mechanics*, Martinus Nijhoff, Dordrecht.
- Kohavi, R. and Quinlan, R. (2002). Decision Tree Discovery, In: Will Klosgen and Jan M. Zytkow (eds), *Hand Book of Data Mining and Knowledge Discovery*, Chapter 16.3.1, Oxford, pp. 267–276, Oxford University Press, New York.
- Kumar, A. and Dawson, P.R. (1998). Modeling Crystallographic Texture Evolution with Finite Elements Over neo-Eulerian Orientation Spaces. *Computer Methods in Applied Mechanics and Engineering*, **153**: 259–302.
- Liu, H.T., Sun, L.Z. and Ju, J.W. (2006). Elastoplastic Modeling of Progressive Interfacial Debonding for Particle-reinforced Metal-matrix Composites, *Acta Mechanica*, **181**(1–2): 1–17.
- Liu, H., Arwade, S.R. and Igusa, T. (2007). Random Composites Classifications and Damage Estimations Using Bayesian Classifiers, *ASCE Journal of Engineering Mechanics*, **133**(2): 129–140.
- Louhghalam, A., Arwade, S.R. and Igusa, T. (2006). Representation of Random Composite Materials Using basis Functions Extracted from Principal Component Analysis, In: *15th US National Congress on Theoretical and Applied Mechanics*, Boulder, CO, June.
- Moes, N., Dolbow, J. and Belytschko, T. (1999). A Finite Element Method for Crack Growth without Remeshing, *International Journal for Numerical Methods in Engineering*, **46**(1): 131–150.
- Ohser, J. and Mücklich, F. (2000). *Statistical Analysis of Microstructures in Material Science*, John Wiley and Sons, West Sussex, England.
- Paulino, G.H., Yin, H.M. and Sun, L.Z. (2006). Micromechanics Based Interfacial Debonding Model for Damage of Functionally Graded Materials with Particle Interactions, *International Journal of Damage Mechanics*, **15**(3): 267–288.
- Pawtucket, R.I. Abaqus Inc. Abaqus version 6.5 users manual ([www.abaqus.com](http://www.abaqus.com))
- Platt, J.C. (1999). Training of Support Vector Machines Using Sequential Minimal Optimization, In: *Advances in Kernel Methods Support Vector Learning*, MIT Press, Cambridge, MA, USA.
- Stoyan, D., Kendall, W.S. and Mecke, J. (1995). *Stochastic Geometry and its Applications*, Wiley, Colchester.
- Sukumar, N., Moes, N., Moran, B. and Belytschko, T. (2000). Extended Finite Element Method for Three-dimensional Crack Modeling, *International Journal for Numerical Methods in Engineering*, **48**(11): 1549–1570.
- Sundararaghavan, V. and Zabarar, N. (2005). Classification and Reconstruction of Three-dimensional Microstructures Using Support Vector Machines, *Computational Materials Science*, **32**: 223–239.
- Tan, L. and Arwade, S.R. (2008). Response Classification of Simple Polycrystalline Microstructures, *Computer Methods in Applied Mechanics and Engineering*, **197**: 1397–1409.

- Tan, P.-N., Steinbach, M. and Kumar, V. (2005). *Introduction to Data Mining*, Addison Wesley.
- Ural, A., Heber, G., Wawrzynek, P.A., Ingreaffea, A.R., Lewicki, D.G. and Neto, J.B.C. (2005). Three Dimensional, Parallel, Finite Element Simulation of Fatigue Crack Growth in a Sprial Bevel Pinion Gear, *Engineering Fracture Mechanics*, **72**(8): 1148–1170.
- Vapnik, V.N. (1998). *Statistical Learning Theory*, Wiley, New York.
- Voyiadjis, G.Z. and Kattan, P.I. (2006). Damage Mechanics with Fabric Tensors, *Mechanics of Advanced Materials and Structures*, **13**(4): 285–301.
- Voyiadjis, G.Z. and Abed, F.H. (2007). Transient Localizations in Metals Using Microstructure-based Yield Surfaces, *Modelling and Simulation in Materials Science and Engineering*, **15**(1): S83–S95.
- Wei, R.P. and Harlow, D.G. (2003). Corrosion-enhanced Fatigue and Multiple Site Damage, *AIAA Journal*, **41**(10): 2045–2050.
- Witten, I.H. and Frank, E. (2005). *Data Mining: Practical Machinelearning Tools and Techniques*, 2nd edn, Morgan Kaufmann, San Francisco.